



Compatibility of big bang nucleosynthesis in some modified gravities

Abdul Malik Sultan^{1,2,a}, Abdul Jawad^{1,b}

¹ Department of Mathematics, COMSATS University Islamabad, Lahore Campus, Lahore 54000, Pakistan

² Department of Mathematics, University of Okara, Okara 56300, Pakistan

Received: 21 May 2022 / Accepted: 23 September 2022

© The Author(s) 2022

Abstract This paper is devoted to investigate the implications of Einstein-Aether and modified Hořava-Lifshitz theories of gravity to the formation of light elements in the early universe named as big bang nucleosynthesis. We choose different models from these theories for a detailed investigation of big bang nucleosynthesis epoch and compare it with the observational bounds. That is, we compare the deviation of freeze-out temperature T_f with the Λ CDM paradigm and use observational bounds on $\left| \frac{\Delta T_f}{T_f} \right|$ to inspect constraints on the involved free parameters of these models. We apply Chi-square test on the Hubble parameter H in each model to analyze the compatibility of model parameters with the observations and find consistent results. We find that chosen models of Einstein-Aether gravity and modified Hořava-Lifshitz gravity can satisfy big bang nucleosynthesis constraints and thus constitute a viable cosmology since they can be source for dark energy sector and late-time accelerated expansion.

1 Introduction

The Λ CDM cosmological model also known as standard cosmological model has been successfully explained the dynamic and evolution of the universe from its beginning (big bang) to the present accelerated phase assuming that Einstein's general relativity (GR) defines gravity. But standard cosmological model has no proofs about dark energy (DE) and dark matter (DM). It is also unable to explain matter-antimatter asymmetry [1]. Researchers are of the opinion on the basis of observational data coming from Supernova Ia [2,3], cosmic microwave background [4,5] and large scale

structure formation [6–8] that presented accelerated expansion of the universe is due the presence of DE. The DE sector commands over the cold dark matter and navigate the universe towards accelerated expansion due to its enough negative pressure [2,9,10].

The evolution of the universe starting with big bang expanded rapidly from its initial singularity and its density exceeded from critical density in $t < 10^{-43}$ seconds (s) called Planck epoch. After that separation between fundamental forces such as gravitational and electro-nuclear forces took place in $t < 10^{-36}$ s followed by a very rapid expansion called inflationary phase completed in $t < 10^{-32}$ s. Hereafter the electroweak force decomposed into the weak nuclear and electromagnetic forces when $t = 10^{-12}$ s and at the same time there was a decrease in the energy density of the universe such that matter can exist in the form of quarks [11].

For physicists, there are many puzzles related to the early universe among which one is the formation of light elements after the explosion. Bethe in 1939 first time presented the idea of big bang nucleosynthesis (BBN) which is also known as primordial nucleosynthesis [12]. It is a prime prediction of big bang cosmology which took place after baryogenesis. Most cosmologists believe that it took place about 10–20 s after the big bang and concluded in just 20 min approximately [13]. It was time when formation of stable neutrons and protons came into exist as universe became cool enough. This cooling allowed protons and neutrons to fuse to become isotopes of Hydrogen 1H and Helium 4He . This phenomenon elaborates the relative abundance of Helium in the universe.

The primordial 4He came into exist when temperature of the cosmos was $T \sim 100$ MeV, while energy and number density were under the effects of relativistic leptons (electrons, protons, neutrinos) and light emitting particles photons (where protons and neutron do not contribute in the total energy density) [14]. These particles remain in thermal

^a e-mails: ams@uo.edu.pk; maliksultan23@gmail.com

^b e-mails: abduljawad@cuilahore.edu.pk; jawadab181@yahoo.com (corresponding author)

equilibrium retaining their collisions, while the following relationships to protons and neutrons with lepton

$$v_e + n \leftrightarrow p + e^-, \quad (1)$$

$$e^+ + n \leftrightarrow p + \bar{v}_e, \quad (2)$$

$$n \leftrightarrow p + e^- + \bar{v}_e, \quad (3)$$

hold the particles in thermal equilibrium (where e represents number of electrons, p describes number of protons, n is number of neutrons and v_e gives number of neutrinos in the system). Moreover, in accelerated universe, the conversion rate of protons into neutrons is used to estimate the neutron abundance.

Moreover, there are some other evolutionary era of the universe which are of much importance such as radiation dominated era, matter dominated era and the formation of large scale structures. In the beginning, after big bang explosion the universe was so hot that energy density of electromagnetic radiation was greater than the density of matter and was driving the expansion called radiation dominated era. It took 47,000 years when energy density of matter overtaken the density of radiation and hence matter became driver of universe's evolution called matter dominated era. Furthermore, the source for the formation of larger structure was smaller structure which came into exist first and built up into the larger structure. Scientists are of the opinion that at $t = 700$ Myr stars (population III stars) come into exist and then dwarf galaxies and quasars yet to be detected observationally [11].

To analyze the historical background and recent picture of universe, the modified theories of gravity have much prominent role as compared to Einstein's GR. The above motivation can be fulfilled by numerous gravitational modifications. Cosmological models which deal with higher-order corrections to the Einstein–Hilbert Lagrangian have additional motivation of improving the renormalizability of GR [15, 16]. These higher-order cosmological models come into exist when an additional term in Einstein–Hilbert action is added such as $f(R)$ gravity [17] with R as Ricci curvature, Weyl gravity [18, 19], Lovelock cosmology [20], Galileon theory of gravity [21, 22], Einstein cubic gravity [23, 24] etc. For current analysis on DE issue including modified theories of gravity, a lot of work have been done in the literature [25–53].

Many physicists worked on constraining BBN under the realm of various cosmological models to analyze the formation of light in early universe. Capozziello et al. [13] used BBN observational bounds on the primordial abundance of photons to constrain $f(T)$ cosmology (where T is torsion scalar) and studied three different models in order to examine BBN constraints on their free parameters. Barrow et al. [54] used BBN observational data to impose the BBN constraints on the exponent Δ of Barrow entropy. Bhattacharjee [55] constrained model $f(Q, T) = Q^{n+1} + mT$ under $f(Q, T)$

gravity (where Q is non-metricity) to investigate the viability in cosmology and found that this cosmological model can explain the observed abundances of Helium and Deuterium while Lithium problem persists. Ghoshal and Lambiase [14] used Tsallis cosmology to examine the bound on Tsallis parameter to be $\beta < 2$ by using the constraints coming from the formation of light element from the BBN observational data which permit a very small deviation from GR. Asimakis et al. [56] used BBN data to impose observational constraints on higher-order modified theories of gravity particularly Gauss–Bonnet $f(G)$ gravity, $f(P)$ cubic gravity and running vacuum gravity. They have given a detailed discussion of BBN epoch and investigated the deviation of freeze-out time with a comparison to Λ CDM regime. They found BBN constraints by using the observational data on involved free parameters of various models.

The aim and motivation of this work is to address the implications of Einstein–Aether and modified Hořava–Lifshitz theories of gravity on BBN which is a source to form the light element in the early universe as the cosmological models are assumed viable if and only if they satisfy some suitable conditions imposed by BBN. Since BBN occurred in first 10–20 s after big bang and completed in approximately twenty minutes when the universe was hot and dense (indeed BBN, together with cosmic microwave background radiation, provides the strong evidence about the high temperatures characterizing the primordial universe). It reports that nuclear reactions happened in a sequence that yield the synthesis of photons [57–59] and therefore drive the observed universe. Thus from BBN physics, one can deduce stringent constraints on a given theory of gravity related models. Hence, in this paper, we shall confront Einstein–Aether and modified Hořava–Lifshitz theories of gravity models with BBN depending upon recent observational data. We shall consider different models related to Einstein–Aether gravity and modified Hořava–Lifshitz theories of gravity that mimic Λ CDM model.

The arrangement of this paper is as follows: In upcoming section, we review the Einstein–Aether and modified Hořava–Lifshitz theories of gravity. In Sect. 3, we calculate the BBN constraints. In Sect. 4, we review the chi-square test and discussed observational values of the Hubble parameter H . In Sect. 5, we analyze BBN in Einstein–Aether gravity. In Sect. 6, we analyze BBN constraints in modified Hořava–Lifshitz gravity. In the last section, we conclude our findings.

2 Modified theories of gravity

In this section, we present two different theories of gravity. The first one is Einstein–Aether gravity in which Lorentz invariance is breakup by unit time like vector field (Aether) [60]. The other one is modified Hořava–Lifshitz gravity also

known as $f(\tilde{R})$ gravity. We consider homogeneous, flat and isotropic FRW universe for which line element is

$$ds^2 = -N^2 dt^2 + a^2 \left(dr^2 + r^2(d\theta^2 + \sin^2 \theta d\phi^2) \right), \quad (4)$$

where N is lapse variable depends on time t (for Einstein-Aether gravity $N = 1$) and $a = a(t)$ is scale factor of the universe [61, 62]. The energy momentum tensor for this model is

$$T_{ab}^m = \rho U_a U_b + p(g_{ab} + U_a U_b), \quad (5)$$

where U_a is the four velocity, ρ is the energy density and p describes pressure of the universe respectively. For both theories, continuity equation is given by $\dot{\rho} + 3H(p + \rho) = 0$, where H is the Hubble parameter. In upcoming subsections, we analyze both theories of gravity separately.

2.1 Einstein-Aether gravity

As it is believed by the physicists that Aether is a physical medium that exists everywhere in this universe homogeneously. It is the medium which is reason to travel the light from one place to the other even in vacuum. Physicists are of the opinion that Aether provides a specific static frame of reference in which every traveling object has absolute relative velocity and is well suitable for Newtonian dynamics. But Einstein in his theory of relativity rejected it by performing various experiments on optics. When the concept of cosmic microwave background come into exists, many scientists considered it as modern form of Aether. Gasperini [63] boosted up the Einstein-Aether theory which is said to be covariant moderation of general relativity [60]. The action of Einstein-Aether theory is given as [64, 65]

$$\mathcal{S} = \int \sqrt{-g} \left(\frac{R}{4\pi G} + \mathcal{L}_{EA} + \mathcal{L}_m \right) d^4x, \quad (6)$$

where g represents the determinant of metric tensor $g^{\mu\nu}$ and G is the gravitational constant. Moreover, \mathcal{L}_m is the Lagrangian density of matter while \mathcal{L}_{EA} is the Lagrangian density for the vector field which can be given by

$$\mathcal{L}_{EA} = \frac{1}{16\pi G} \left(M^2 F(K) + \lambda(A^a A_a + 1) \right), \quad (7)$$

where M is a coupling constant, λ referred as Lagrangian multiplier and A^a is a vector (tensor of rank one) to have time-like direction which satisfies the relation $A^a A_a = -1$. Furthermore, $F(K)$ is an arbitrary function involved due to theory with argument K which is given by

$$K = \frac{K_{cd}^{ab} \nabla_a A^c \nabla_b A^d}{M^2}, \quad (8)$$

$$K_{cd}^{ab} = c_1 g^{ab} g_{cd} + c_2 g_c^a g_d^b + c_3 g_d^a g_c^b, \quad a, b = 0, 1, 2, 3, \quad (9)$$

where c_1, c_2, c_3 are constants without dimensions. Einstein field equations for this theory can be obtained from Eq. (6) as

$$G_{ab} = T_{ab}^{EA} + 8\pi G T_{ab}^m, \quad (10)$$

$$\nabla_a \left(F' J_b^a \right) = 2\lambda A_b, \quad (11)$$

where prime denotes the derivative w.r.t the argument K , T_{ab}^m is the energy momentum tensor for matter field and is given in Eq. (5), $J_b^a = -2K_{bc}^{ad} \nabla_d A^c$ and T_{ab}^{EA} represents energy momentum-tensor for vector field which is given by

$$T_{ab}^{EA} = \lambda A_a A_b + \frac{g_{ab} M^2 F}{2} - Y_{(ab)} F' + \frac{1}{2} \nabla_d \left[\left(J_{(a}^d A_{b)} - J^d_{(a} A_{b)} - J_{(ab)} A^d \right) F' \right], \quad (12)$$

where indices (ab) represents symmetry, A_a is time-like unitary vector and is defined as $A_a = (1, 0, 0, 0)$ and $Y_{(ab)}$ is given as

$$Y_{(ab)} = -c_1 [(\nabla_d A_a)(\nabla^d A_b) - (\nabla_a A_a)(\nabla_b A_d)]. \quad (13)$$

The Friedmann equations for Einstein-Aether theory of gravity become

$$\gamma \left(\frac{1}{2} F K^{-1} - F' \right) H^2 + \left(\frac{K}{a^2} + H^2 \right) = \frac{8\pi G}{3} \rho, \quad (14)$$

$$\gamma \left(\dot{H} F' + H \frac{dF'}{dt} \right) + \left(\frac{2K}{a^2} - 2\dot{H} \right) = 8\pi G(\rho + p), \quad (15)$$

where overhead dot means derivative w.r.t cosmic time ‘ t ’, the constant parameter $\gamma = c_1 + 3c_2 + c_3$ and the argument $K = \frac{3\gamma H^2}{M^2}$. If ρ_{EA} is the effective energy density and p_{EA} is the effective pressure in Einstein-Aether gravity then Eqs. (14) and (15) becomes as

$$\left(\frac{K}{a^2} + H^2 \right) = \frac{8\pi G}{3} \rho + \frac{1}{3} \rho_{EA}, \quad (16)$$

$$\left(\frac{2K}{a^2} - 2\dot{H} \right) = 8\pi G(\rho + p) + (\rho_{EA} + p_{EA}), \quad (17)$$

where

$$\rho_{EA} = 3\gamma H^2 \left(F' - \frac{1}{2} F K^{-1} \right), \quad (18)$$

$$p_{EA} = -\gamma \left(\dot{H} F' + H \frac{dF'}{dt} \right) - 3\gamma H^2 \left(F' - \frac{F}{2K} \right). \quad (19)$$

2.2 Modified Hořava–Lifshitz gravity

In this subsection, we will discuss the modified Hořava–Lifshitz gravity. The generalized action term for this gravity is [61, 66]

$$S_{F(\tilde{R})} = \int d^4x \sqrt{-g} F(\tilde{R}) + S_m, \quad (20)$$

where $\sqrt{-g} = \sqrt{g^{(3)}}N$ and S_m is the matter part of action. Also,

$$\tilde{R} = K_{ab}K^{ab} - \lambda K^2 + 2\mu \nabla_\sigma (n^\sigma \nabla_\nu n^\nu - n^\nu \nabla_\nu n^\sigma) - \mathcal{L}_R^{(3)}(g_{ab}^{(3)}), \quad (21)$$

where μ, λ are real numbers, $\mathcal{L}_R^{(3)}$ is a function depending on three dimensional metric $g_{ab}^{(3)}$ and the covariant derivatives $\nabla_a^{(3)}$ are defined by the metric given in Eq. (4). In this scenario the argument \tilde{R} takes the form

$$\tilde{R} = \frac{(3-9\lambda)H^2}{N^2} + \frac{6\mu}{a^3 N} \frac{d}{dt} \left(\frac{H a^3}{N} \right). \quad (22)$$

The argument \tilde{R} reduces to R and hence usual $f(R)$ -gravity is obtained if we choose parameters $\lambda = \mu = 1$ with flat FRW metric. If we select $\mu = 0$, \tilde{R} reduces to R_{HL} (Ricci scalar for Hořava–Lifshitz gravity) [66] and thus action (20) becomes similar to the action term of Hořava–Lifshitz-like $f(R)$ -gravity [67]. Hence, this assumption ($\mu = 0$) corresponds to some degenerate limit of general $f(R)$ Hořava–Lifshitz gravity. We call this limit degenerate as it is very difficult to obtain (might be impossible).

Considering FRW cosmology for action (20) for which the spatial curvature $R_{ab}^{(3)} = R^{(3)}$ vanishes and thus, $\mathcal{L}_R^{(3)}$ does not contribute any thing (same FRW cosmology obtained for any choice of $\mathcal{L}_R^{(3)}$). It is obvious that this situation varies when black hole or solutions with non-trivial dependence are considered. Suppose that universe is composed with perfect fluid, by varying (20) w.r.t $g_{ab}^{(3)}$ and setting $N = 1$, the Friedmann equations for modified Hořava–Lifshitz gravity are given by

$$\rho = F(\tilde{R}) - 6 \left[(1-3\lambda+3\mu)H^2 + \mu \dot{H} \right] F'(\tilde{R}) + 6\mu H \frac{dF'(\tilde{R})}{dt} - ca^{-3}, \quad (23)$$

$$p = -F(\tilde{R}) + 2 \left[(1-3\lambda+3\mu)(\dot{H} + 3H^2) \right] F'(\tilde{R}) + 2(1-3\lambda)H \frac{dF'(\tilde{R})}{dt} - 2\mu \frac{d^2F'(\tilde{R})}{dt^2}, \quad (24)$$

where prime denotes the derivative of respective function with respect to argument. Here c is the constant of integration and the term ca^{-3} represents the dark matter part when $c > 0$ [68]. As during BBN, dark matter part vanishes (i.e. $c = 0$) [66], therefor Friedmann equations (23) and (24) become

$$\rho_{DE} = F(\tilde{R}) - 6 \left[(1-3\lambda+3\mu)H^2 + \mu \dot{H} \right] F'(\tilde{R}) + 6\mu H \frac{dF'(\tilde{R})}{dt}, \quad (25)$$

$$\rho_{DE} = p. \quad (26)$$

The value of argument \tilde{R} from Eq. (22) reduces to

$$\tilde{R} = 3(1-3\lambda+6\mu)H^2 + 6\mu \dot{H}. \quad (27)$$

3 BBN constraints: basic scenario

In this section, we will develop the relation for deviation of freeze-out time T_f and BBN constraints. Since BBN noticed in radiation era [58, 69, 70], thus during BBN for standard model radiation in context of GR, the first Friedmann equation can be approximated as

$$H^2 \approx \frac{\rho_r}{3M_p^2} = H_{GR}^2, \quad (28)$$

where $M_p = \frac{1}{\sqrt{8\pi G}}$ is reduced Planck mass, ρ_r is energy density of a relativistic particles filling the universe and is given as

$$\rho_r = \frac{\pi^2 g_* T^4}{30}. \quad (29)$$

Here T represents the temperature and $g_* = g(T)$ is the effective number of the degree of freedom usually approximated as $g_* \sim 10$. Substituting the values of ρ_r and M_p in Eq. (28), we get

$$H(T) = \left(\frac{4\pi^3 g_*}{45} \right)^{\frac{1}{2}} \frac{T^2}{M_{p\ell}}, \quad (30)$$

where $M_{p\ell} = \sqrt{8\pi} M_P$ is referred to as Plank mass. Due to radiation conservation, the scale factor of universe evolves as $a(t) \sim \sqrt{t}$, where t is the cosmic time. The Hubble parameter H in terms of cosmic time t becomes as $H = \frac{1}{2t}$ which leads to relation between temperature T and cosmic time t as $\frac{1}{t} = \left(\frac{16\pi^3 g_*}{45} \right)^{\frac{1}{2}} \frac{T^2}{M_{p\ell}}$ (or $T(t) \simeq (t/s)^{-1/2}$ MeV). Since number of neutron arises during BBN due to conversion of some protons-neutron rate [70, 71] which is given as

$$\Lambda_{pn}(T) = \Lambda_{(n+\nu_e \rightarrow p+e^-)} + \Lambda_{(n+e^+ \rightarrow p+\bar{\nu}_e)} + \Lambda_{(n \rightarrow p+e^- + \bar{\nu}_e)}, \quad (31)$$

and its inverse $\Lambda_{np}(T)$. Thus the total rate can be given as $\Lambda_{tot}(T) = \Lambda_{pn}(T) + \Lambda_{np}(T)$. Considering all these particles at same temperature which is low enough causes to use Boltzmann distribution instead of the Fermi-Dirac distribution. Assuming electron mass negligible as compared to electron and neutrino energies, some simple mathematics can be used to calculate neutron abundance via conversion rate of proton into neutron which gives the relation for total rate as [13, 54, 72, 73]

$$\Lambda_{tot}(T) = 8(12T^2 + 6QT + Q^2)AT^3, \quad (32)$$

where Q is the mass difference between neutron and proton given as $Q = m_n - m_p = 1.29 \times 10^{-3}$ GeV and $A = 1.02 \times 10^{-11}$ GeV $^{-4}$. The relation $Y_p = \lambda \frac{2x(T_f)}{1+x(T_f)}$, where $\lambda = e^{(T_f - T_n)/\tau}$ with T_f means freeze-out of weak interaction while T_n represents the farsee-out of nucleosynthesis, $x(T_f) = e^{-\frac{Q}{\tau(T_f)}}$ gives the neutron to proton equilibrium ratio and $\tau = 8803 \pm 1.1$ s is the neutron average life time [74]. Moreover, the function $\lambda(T_f)$ represents the portion of neutrons that decay into proton in the interval $[T_f, T_n]$. Now we compare the universe expansion rate H^{-1} and the function $\Lambda_{tot}(T)$ given in (32) to calculate the freeze-out time T_f . We can consider system in thermal equilibrium if interaction time is much larger then expansion time (i.e. $H^{-1} \ll \Lambda_{tot}(T)$) [57, 69]. On the other hand, the particles decouple if expansion time is much larger then interaction time (i.e. $H^{-1} \gg \Lambda_{tot}(T)$). The temperature during which decoupling takes place is freeze-out temperature T_f that corresponds to $H(T_f) = \Lambda(T_f) \simeq c_q T_f^5$, where $c_q \equiv 96A \simeq 9.8 \times 10^{-10}$ GeV $^{-4}$ [13, 54, 72, 73]. Using Eqs. (30) and (32), above requirement leads to the relation

$$T_f = \left(\frac{4\pi^3 g_*}{45c_q^2 M_{p\ell}^2} \right)^{1/6}. \quad (33)$$

The Hubble parameter H will deviate from H_{GR} in context of modified cosmology, due to which freeze-out time also presents a deviation ΔT_f from (28). Due to this deviation in fractional mass, Y_p is given as

$$\Delta Y_p = Y_p \left[\left(1 - \frac{Y_p}{2\lambda} \right) \ln \left(\frac{2\lambda}{Y_p} - 1 \right) - \frac{2T_f}{\tau} \right] \frac{\Delta T_f}{T_f}, \quad (34)$$

where we take $\Delta T(T_n) = 0$ as T_n is fixed by deuterium binding energy [72, 73, 75]. During BBN era, the observational estimation of mass fraction is [76–81]

$$Y_p = 0.2476, \quad |\Delta Y_p| < 10^{-4}. \quad (35)$$

One can obtain an extra term in Friedmann equations by using any modified theories of gravity which needs to be small compared to the radiation sector of standard cosmology during BBN era so that observational facts may not be spoiled. Thus, from the general modified Friedmann equation, $3M_p^2 H^2 = \rho_m + \rho_r + \rho_{DE}$, we can obtain

$$H = H_{GR} \left(1 + \frac{\rho_{DE}}{\rho_r} \right)^{1/2} = \Delta H + H_{GR}, \quad (36)$$

where $H_{GR} = M_p \sqrt{\frac{\rho_r}{2}}$ is the rate at which universe expands in standard cosmology. Thus, we obtain

$$\Delta H = H_{GR} \left(\sqrt{1 + \frac{\rho_{DE}}{\rho_r}} - 1 \right). \quad (37)$$

This deviation from standard cosmology will lead to a deviation in the freeze-out temperature ΔT_f . Since $H_{GR} = \Lambda_{tot} \approx c_q T_f^5$. This relation along with (33) leads to the relation

$$H_{GR} \left(\sqrt{1 + \frac{\rho_{DE}}{\rho_r}} - 1 \right) = 5c_q T_f^4 \Delta T_f. \quad (38)$$

In the regime $\rho_{DE} \ll \rho_r$, one can find finally

$$\frac{\Delta T_f}{T_f} \simeq \frac{\rho_{DE}}{\rho_r} \frac{H_{GR}}{10c_q T_f^5}. \quad (39)$$

The above theoretically evaluated relation should be compared with the following observational bound

$$\left| \frac{\Delta T_f}{T_f} \right| < 4.7 \times 10^{-4}, \quad (40)$$

which is found by using observation estimation of the baryon mass fraction converted into 4He [76–81] which is given in Eq. (35).

4 Chi-square test

A statistical test Chi-square developed by Pearson in 1900 [82] is used for a comparison between the observed values and expected values. Pearson also applied it to test the goodness of fit for frequency curves. This test exhibits, whether the difference between two data sets is due to chance or due to relationship of variables under consideration. The condition to perform Chi-square test is that data set must have points more than five. The outcome of Chi-square test is a single number which analyze the difference between the observed values and expected values of the data sets. There is no difference between two data sets (data sets are identical) if the value of Chi-square is zero. A larger value of χ^2 exhibits bigger difference between the two data sets as compared to a smaller value of χ^2 . To evaluate the limit and best fitting values for different models, we use the χ^2 static as

$$\chi^2(p) = \sum \left(\frac{O_i - E_i}{\sigma_i} \right)^2, \quad (41)$$

where i counts the data points, O_i represents the observed value, E_i is the corresponding expected value, σ_i is the error associated with i th observed value in the data and p denotes the set of model parameters. To observe the compatibility of models with the recent observational data, we will calculate the Hubble parameter H for each model in upcoming sections and compare the corresponding values of H with recent data. Bhardwaj et al. [83] presented the observed values of H for 46 different points against redshift parameter z along with their observational error evaluated by using various age approach by different cosmologists presented in the Table 1 as

Table 1 The behavior of Hubble parameter H against redshift parameter z [83]

S.No	z	$H(Obs)$	σ_i	References	S.No	z	$H(Obs)$	σ_i	References
1	0	67.77	1.30	[84]	2	0.07	69	19.6	[85]
3	0.09	69	12	[86]	4	0.1	69	12	[87]
5	0.12	68.6	26.2	[85]	6	0.17	83	8	[87]
7	0.179	75	4	[88]	8	0.1993	75	5	[88]
9	0.2	72.9	29.6	[85]	10	0.24	79.7	2.7	[89]
11	0.27	77	14	[87]	12	0.28	88.8	36.6	[85]
13	0.35	82.7	8.4	[90]	14	0.352	83	14	[88]
15	0.38	81.5	1.9	[91]	16	0.3802	83	13.5	[90]
17	0.4	95	17	[86]	18	0.4004	77	10.2	[92]
19	0.4247	87.1	11.2	[92]	20	0.43	86.5	3.7	[89]
21	0.44	82.6	7.8	[93]	22	0.44497	92.8	12.9	[92]
23	0.47	89	49.6	[94]	24	0.4783	80.9	9	[92]
25	0.48	97	60	[87]	26	0.51	90.4	1.9	[91]
27	0.57	96.8	3.4	[95]	28	0.593	104	13	[88]
29	0.60	87.9	6.1	[93]	30	0.61	97.3	2.1	[91]
31	0.68	92	8	[88]	32	0.73	97.3	7	[93]
33	0.781	105	12	[88]	34	0.875	125	17	[88]
35	0.88	90	40	[87]	36	0.9	117	23	[87]
37	1.037	154	20	[89]	38	1.3	168	17	[87]
39	1.363	160	33.6	[96]	40	1.43	177	18	[87]
41	1.53	140	14	[87]	42	1.75	202	40	[96]
43	1.965	186.5	50.4	[89]	44	2.3	224	8	[97]
45	2.34	222	7	[98]	46	2.36	226	8	[99]

5 BBN of various models in Einstein-Aether gravity

In this section, we apply the formalism obtained in the Sect. 3 to find the BBN constraints under the realm of Einstein-Aether gravity. We use DE relation (18) which holds in the contexts of Einstein-Aether gravity to find the BBN constraints as well as the Hubble parameter H . We will focus on three different models to examine the BBN constraints and Hubble parameter.

5.1 Model 1

The first model which we use to inspect BBN constraints in context of Einstein-Aether gravity is

$$F(K) = f_0 K^n, \quad K > 0, \quad (42)$$

where f_0 is a positive constant as cosmic acceleration is observed only for $f_0 > 0$ [100] and n is the only free parameter. Moreover, f_0 can be expressed in terms of H_0 (i.e. present value of Hubble parameter) as $n \neq 1$. The present value of DE density can be given as

$$\Omega_{DE0} = \frac{\rho_{DE0}}{3M_p^2 H_0^2}, \quad (43)$$

where Ω_{DE0} is the current matter density parameter and is approximately equivalent to 0.7 while

$$H_0 = 73.02 \pm 1.79 \text{ km/(sMpc)}, \\ \sim 2.1 \times 10^{-42} \text{ GeV}.$$

is the Hubble parameter at present [13]. The best fit on other free parameters can be obtained by taking the CC + H_0 + SNeIa + BAO observational data [101]. During BBN era, assuming $\rho_{DE} = \rho_{DE0}$ and inserting its value along with $F(K)$ in Eq. (18), we get

$$f_0 = \frac{2M_p^2 \Omega_{DE0} \left(\frac{\gamma H_0^2}{M^2} \right)^{1-n}}{3^{n-1} (2n-1) \gamma}. \quad (44)$$

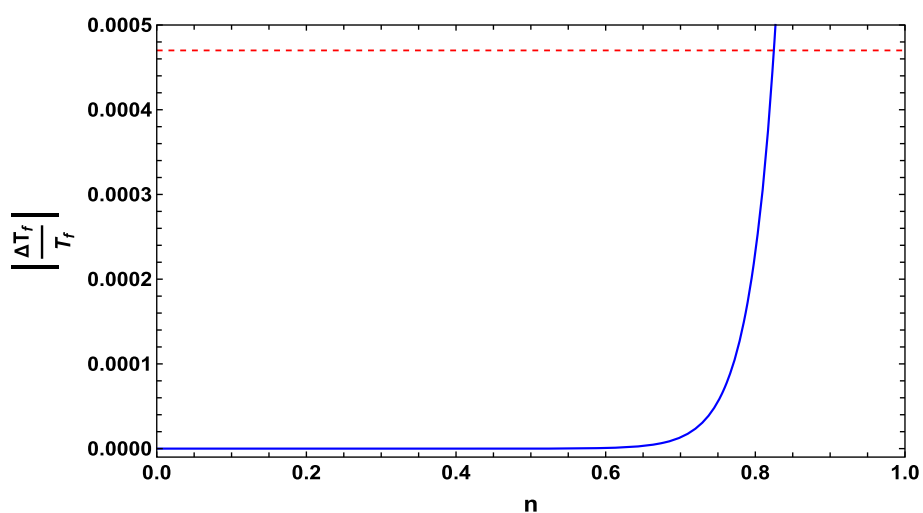
Inserting Eq. (42) along with (44) into (18) and then simplifying (39), we have

$$\frac{\Delta T_f}{T_f} = \frac{\Omega_{DE0} H_0^{2-2n} \xi^{2n-1} T_f^{4n-7}}{10c_q}, \quad (45)$$

where T_f is given in (33) and

$$\xi = \frac{1}{M_p \ell} \left(\frac{4\pi^3 g_*}{45} \right)^{\frac{1}{2}}. \quad (46)$$

Fig. 1 Variation of $\left| \frac{\Delta T_f}{T_f} \right|$ given in Eq. (45) against free parameter n



We depict $\left| \frac{\Delta T_f}{T_f} \right|$ in Fig. 1 against the free parameter n appearing in (45) with an upper bound coming in (40). It can be observed from the figure that the mathematical relation (45) satisfies the bound (40) for $n \leq 0.8247$. The fixed parameters to plot (45) are chosen as $H_0 = 0.69$, $\gamma = 1$, $\Omega_{DE0} = 0.7$ and $M = 5$. It is of great interest that under the requirement, Einstein-Aether gravity describes DE at late universe, conditions (44) must be satisfied. If n is restricted near zero then constraint given in Eq. (39) becomes constant which describes Λ CDM regime. To observe the compatibility of model with observations, we insert the value of $\rho = \rho_0 a^{-3(1+\omega)}$ where $\rho_0 = 3M_p^2 H_0^2 \Omega_{DE0}$ from continuity equation and ρ_{EA} from Eq. (18) in Eq. (16), we have

$$2H^2 + (\gamma F K^{-1} - 2\gamma F')H^2 = \frac{16\pi G}{3} \rho_0 a^{-3(1+\omega)} - \frac{2K}{a^2}, \quad (47)$$

where $8\pi G = 1$. Substituting the values of F , F' , K in the above equation and using the transformation from cosmic time t to the redshift parameter z given as $\frac{dH}{dt} = -(1+z)H \frac{dH}{dz}$, simplification leads to the relation

$$H'(z) = \frac{3H_0^2 \Omega_{DE0} (\omega + 1)(z + 1)^{3\omega + 2} M^2 - 6\gamma(z + 1)H^2}{f_0 3^{n-1} n (1 - 2n) \gamma^n M^{4-2n} H(z)^{2n-1} + 6\gamma(z + 1)^2 H(z) + 2H(z)M^2}. \quad (48)$$

The above equation is a complicated first order ordinary differential equation from which it is difficult to obtain the exact solution. To overcome this complexity, we solve the above equation numerically by using the software mathematica and extract the 43 different values of H against z given in serial number 1 to 43 in Table 1 and plots are in Fig. 2. The error bars representing observations given in [83] are also added to the figure for comparison. Our estimated values for various cosmological parameters for minimum χ^2 are computed $H_0 = 0.69$, $M = 5$, $\gamma = 1$, $\omega = -1/3$, $\Omega_{DE0} = 0.7$ which are identical to the values used to plot Fig. 1 with five

different values of n mentioned in the panel of Fig. 2. The values of χ^2 obtained for different values of n are as follows

$$\chi^2 = \begin{cases} 224.9193 & \text{for } n = 1.080, \\ 152.3425 & \text{for } n = 1.085, \\ 176.7795 & \text{for } n = 1.090, \\ 224.0224 & \text{for } n = 1.095, \\ 271.6758 & \text{for } n = 1.100. \end{cases}$$

The Chi-square analysis (to test the goodness of fit for the curves) depicts that the obtained results are closed to the observations when $n = 1.085$ and differ utmost from the observational data when $n = 1.1$. Moreover, the values of model parameters which are estimated to analyze the BBN compatibility are best fit according to χ^2 test.

5.2 Model 2

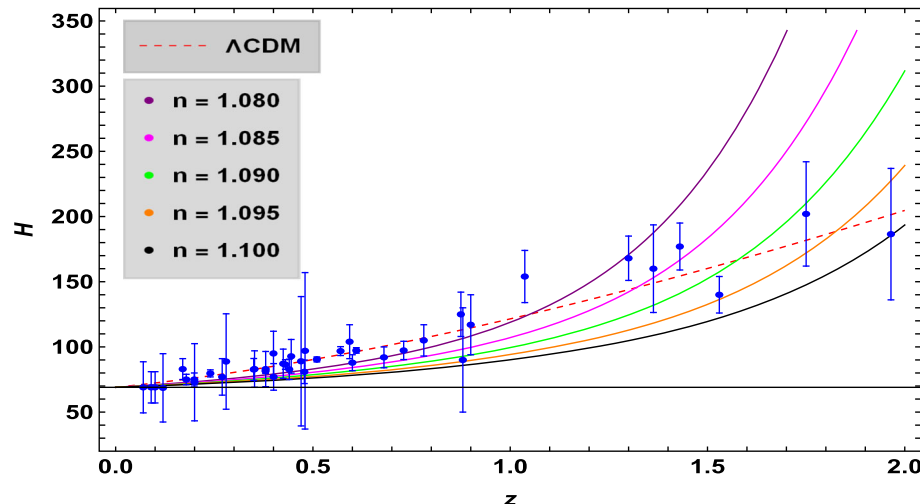
The second model which we inspect for BBN constraints under the realm of Einstein-Aether gravity is given as

$$F(K) = \alpha K^n + \beta, \quad (49)$$

where α and $\beta \neq 0$ are real constants. This model is more generalized as the model given in (42) and reduces to the model (42) if we choose $\beta = 0$. We can find mathematical relation for the constant α for BBN era as

$$\alpha = \frac{M^{2(n-1)} [\beta M^2 + 6H_0^2 M_p^2 \Omega_{DE0}]}{M^2 (2n - 1)}. \quad (50)$$

Fig. 2 The evolution of the Hubble parameter H against redshift z for different values of $n = 1.08$ (purple), 1.085 (magenta), 1.09 (green), 1.095 (orange), 1.1 (black). The dashed red line relates to the Λ CDM model. The error bars represent the observational values. We consider that $H_0 = 0.69$, $M = 5$, $\gamma = 1$, $\omega = -1/3$, $\Omega_{DE0} = 0.7$ and f_0 is given in Eq. (44)



Substituting Eq. (49) along with (50) into (18) and then simplifying for the constraints given in (39), we have

$$\left| \frac{\Delta T_f}{T_f} \right| = \frac{\xi^{2n} T_f^{4n} (\beta M^2 + 6H_0^2 M_p^2 \Omega_{DE0}) - \beta M^2 H_0^{2n}}{60c_q M_p^2 H_0^{2n} \xi T_f^7}. \quad (51)$$

We plot $\left| \frac{\Delta T_f}{T_f} \right|$ versus n in Fig. 3 appearing in Eq. (51) with an upper bound coming in (40). We have chosen the fixed constants as $H_0 = 0.69$, $\beta = 0.6$ and $M = 5$. It can be observed from the figure that the mathematical relation (51) satisfies the bound (40) for $n \leq 0.7498$. Moreover, if we restrict the free parameter n near zero, then the bound coming in (39) becomes constant which justify the Λ CDM regime. For comparison with recent observational data, we substitute ρ with from continuity equation and ρ_{EA} from Eq. (18) in Eq. (16), we have

$$2H^2 + \beta\gamma K^{-1}H^2 + \alpha\gamma K^{n-1}(1-2n)H^2 = \frac{2}{3}\rho_0 a^{-3(1+\omega)} - \frac{2K}{a^2}. \quad (52)$$

Substituting the corresponding values in the above equation and using the transformation from t to z , simplification leads to the equation

$$H'(z) = \frac{3H_0^2 \Omega_{DE0}(\omega+1)(z+1)^{3\omega+2}M^2 - 6\gamma(z+1)H^2}{3^{n-1}n\alpha(1-2n)\gamma^n M^{4-2n}H(z)^{2n-1} + 6\gamma(z+1)^2H(z) + 2H(z)M^2}. \quad (53)$$

We solved the above equation numerically using the software mathematica due to its complexity and extracted 43 different values of Hubble parameter H for various values of z given in serial number 1 to 43 in Table 1 and plotted in Fig. 4. The error bars added to the figure for comparison representing observations given in [83]. The estimated values for different parameters for minimum χ^2 have been computed as $n = 1.096$, $M = 5$, $\beta = 0.6$, $\gamma = 1$, $\omega = -1/3$, $\Omega_{DE0} = 0.7$ and α is given in Eq. (50) which are similar to the values

chosen to plot Fig. 3. The values of χ^2 obtained for different values of H_0 are as follow

$$\chi^2 = \begin{cases} 473.4646 & \text{for } H_0 = 64, \\ 277.9502 & \text{for } H_0 = 68, \\ 157.3789 & \text{for } H_0 = 72, \\ 110.8029 & \text{for } H_0 = 76, \\ 139.4633 & \text{for } H_0 = 80. \end{cases}$$

With five different values of H_0 mentioned in the panel, the goodness of fit (χ^2) for the curves shows that it is least for the curve having $H_0 = 76$ which is closest value to observations and most difference occur with the observations when $H_0 = 64$. The χ^2 test exhibits that model parameters estimated to analyze BBN consistency are best fit compared to the observational data and the Λ CDM regime.

5.3 Model 3

The third model which we assume to investigate BBN constraints under the realm of Einstein-Aether gravity is much more generalized as compared to both of the previous models and is given as

$$F(K) = K + \alpha K^2 + \beta K^n, \quad K > 0, \quad (54)$$

where α and β are real constants. As in BBN era, DM does not exist. Thus the mathematical relation for constant β in BBN era can be obtained as

$$\beta = -\frac{M^{2n} (9\alpha\gamma^2 H_0^2 + M^2(\gamma - 2M_p^2 \Omega_{DE0}))}{(2n-1)3^{n-1}H_0^{2(n-1)}\gamma^n M^4}. \quad (55)$$

Fig. 3 Variation of $\left| \frac{\Delta T_f}{T_f} \right|$ given in Eq. (51) against free parameter n

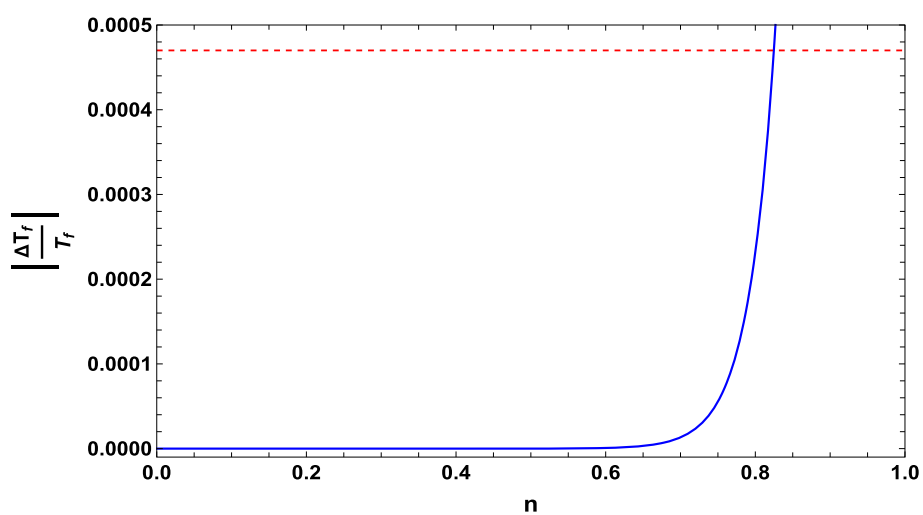
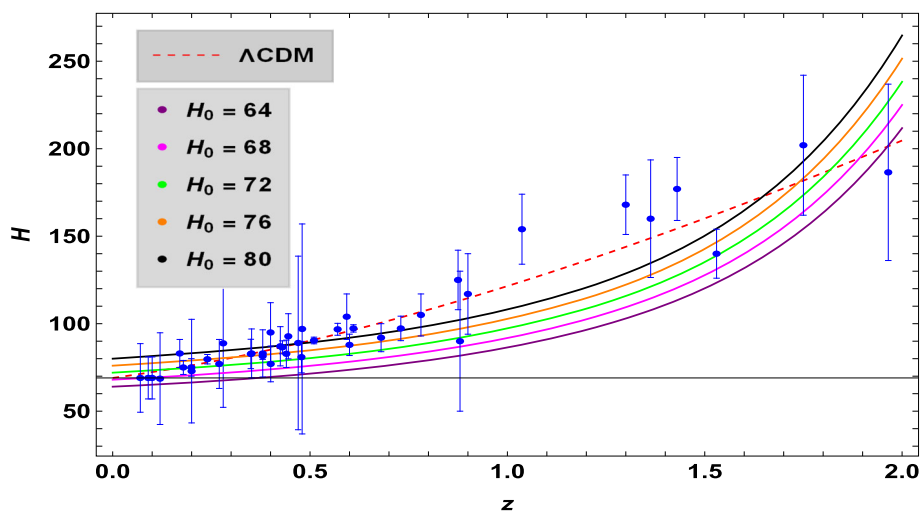


Fig. 4 Hubble parameter versus redshift error bar plot comparing with Λ CDM



Inserting Eqs. (54) and (55) into (18), the simplification of Eq. (39) yields

$$\frac{\Delta T_f}{T_f} = \frac{\gamma H_0^{2(n-1)} (M^2 + 9\alpha\xi^2 T_f^4 \gamma) - \xi^{2n-1} T_f^{4n-4} (9\alpha H_0^2 \gamma^2 + M^2 (\gamma - 2M_p^2 \Omega_{DE0}))}{20M^2 c_q M_p^2 T_f^3 H_0^{2(n-1)}}. \quad (56)$$

Figure 5 describes the graph of above equation against the free parameter n having an upper bound 4.7×10^{-4} . It is easy to observe from the Fig. 5 that the absolute value of above mathematical relation remains less than the upper bound (4.7×10^{-4}) when $n \leq 0.8071$. The other fixed parameters are chosen as $H_0 = 0.69$, $\gamma = 0.002$, $\alpha = 10^{-9}$ and $M = 5$. Moreover, the bound existing in Eq. (39) becomes constant if we restrict the free parameter n near

zero which favors the Λ CDM regime. For comparison with recent observational data, we substitute $\rho = \rho_0 a^{-3(1+\omega)}$ with

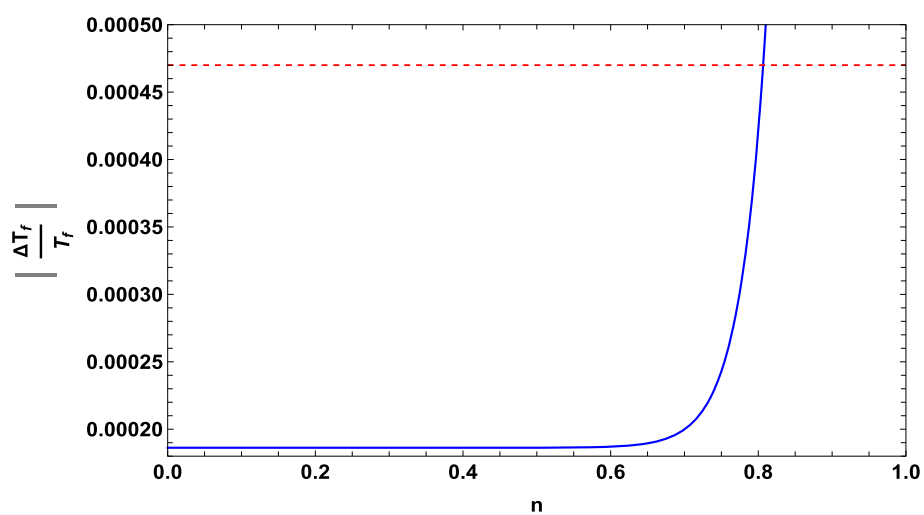
$\rho_0 = 3M_p^2 H_0^2 \Omega_{DE0}$ from continuity equation and ρ_{EA} from Eq. (18) in (16), we have

$$2H^2 + \frac{3\alpha\gamma^2 H^4}{M^2} - \gamma H^2 - \frac{6\alpha\gamma^2 H^4}{M^2} + \frac{3^{n-1} \beta \gamma^n H^{2n} (1-2n)}{M^{2n-2}} = \frac{2}{3} \rho_0 a^{-3(1+\omega)} - \frac{6\gamma H^2}{M^2 a^2}. \quad (57)$$

Using the transformation from t to z and differentiating w.r.t. redshift z , simplification leads to the relation

$$H'(z) = \frac{3H_0^2 M^2 (\omega + 1) \Omega_{DE0} (z+1)^{3\omega+2} - 6\gamma (z+1) H^2}{6\gamma (z+1)^2 H - 6\alpha\gamma^2 H^3 + (2-\gamma) H M^2 + \beta 3^{n-1} n (1-2n) \gamma^n H^{2n-1} M^{4-2n}}. \quad (58)$$

Fig. 5 Variation of $\left| \frac{\Delta T_f}{T_f} \right|$ given in (56) against free parameter n for the model $F(K) = K + \alpha K^2 + \beta K^n$ in Einstein-Aether cosmology



We proceed the above equation numerically by using mathematica software as it is a complex first order differential equation and extracted 43 different values of Hubble parameter H for various values of z given in serial number 1 to 43 in Table 1 and plot is in Fig. 6. The error bars representing the recent observational data given in [83] are also added to the figure for comparison. The estimated values for different parameters for minimum χ^2 are computed as $H_0 = 0.69$, $\alpha = 10^{-9}$, $M = 1.2$, $\gamma = 0.002$, $\omega = -1/3$, $\Omega_{DE0} = 0.7$ with five different values of $n = 1.0358$ (purple), 1.0362 (magenta), 1.0366 (green), 1.037 (orange), 1.0374 (black). The values of χ^2 obtained for different values of n are as follows

$$\chi^2 = \begin{cases} 48.9366 & \text{for } n = 1.0358, \\ 122.6629 & \text{for } n = 1.0362, \\ 147.6971 & \text{for } n = 1.0366, \\ 207.2323 & \text{for } n = 1.0370, \\ 260.3635 & \text{for } n = 1.0374. \end{cases}$$

The Chi-square analysis depicts that the values of Hubble parameter are closed to the observations when $n = 1.0358$ and differ utmost from the observational data when $n = 1.0374$. It can be seen from the χ^2 analysis that the model parameters estimate best to analyze BBN compatibility with the observational data and the Λ CDM regime.

6 BBN in modified Hořava–Lifshitz gravity

In this section, we use the formalism to impose the BBN constraints obtained in Sect. 3 under the realm of modified Hořava–Lifshitz gravity. We use DE relation (25) which holds in context of modified Hořava–Lifshitz gravity. We will concentrate on distinct models to examine the BBN constraints.

6.1 Model 1

The first model with which we inspect BBN constraints in context of modified Hořava–Lifshitz gravity is given as

$$F(\tilde{R}) = \alpha \tilde{R}^n, \quad (59)$$

where α is a real constant and \tilde{R} is given in (27). Since DM does not exist during BBN era, we can get expression for the constant α as

$$\alpha = -\frac{H_0^2 M_p^2 \Omega_{DE0} (3\lambda - 2\mu - 1) (H_0^2 (-3\lambda + 2\mu + 1))^{-n}}{3^{n-1} [1 - 3\lambda + 2\mu + 2n(3\lambda + \mu - 2\mu n - 1)]}. \quad (60)$$

Inserting Eqs. (59) and (60) into (25), the simplification of Eq. (39) yields

$$\frac{\Delta T_f}{T_f} = \frac{\Omega_{DE0} T_f^{4n-7} \xi^{2n-1}}{10 c_q H_0^{2n-2}}. \quad (61)$$

Figure 7 describes the graph of $\left| \frac{\Delta T_f}{T_f} \right|$ against the free parameter n having an upper bound 4.7×10^{-4} . It is easy to observe from the figure that the mathematical relation (61) satisfies the bound (40) for $n \leq 0.8246$. The other fixed parameters are chosen as $H_0 = 69$, $H'(0) = 1$, $\lambda = 0.31$, $\omega = -1/3$, $\Omega_{DE0} = 0.7$ and $\mu = 0.009$. Moreover, the bound existing in Eq. (39) becomes constant if we restrict the free parameter n near zero which favors the Λ CDM regime. For comparison with recent observational data, we substitute $\rho = \rho_0 a^{-3(1+\omega)}$ with $\rho_0 = 3M_p^2 H_0^2 \Omega_{DE0}$ from continuity equation and \tilde{R} from Eq. (27) in Eq. (25), we have

$$\begin{aligned} 2H^2 + \frac{3\alpha\gamma^2 H^4}{M^2} - \gamma H^2 - \frac{6\alpha\gamma^2 H^4}{M^2} \\ + \frac{3^{n-1} \beta \gamma^n H^{2n} (1 - 2n)}{M^{2n-2}} \\ = \frac{2}{3} \rho_0 a^{-3(1+\omega)} - \frac{6\gamma H^2}{M^2 a^2}. \end{aligned} \quad (62)$$

Fig. 6 The evolution of the Hubble parameter H against redshift z for different values of n along with the Λ CDM model and the error bars representing the observational values

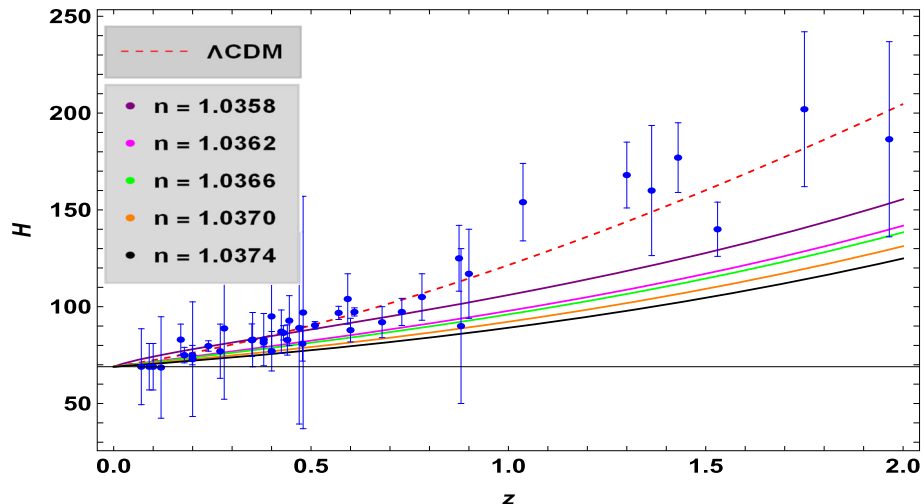
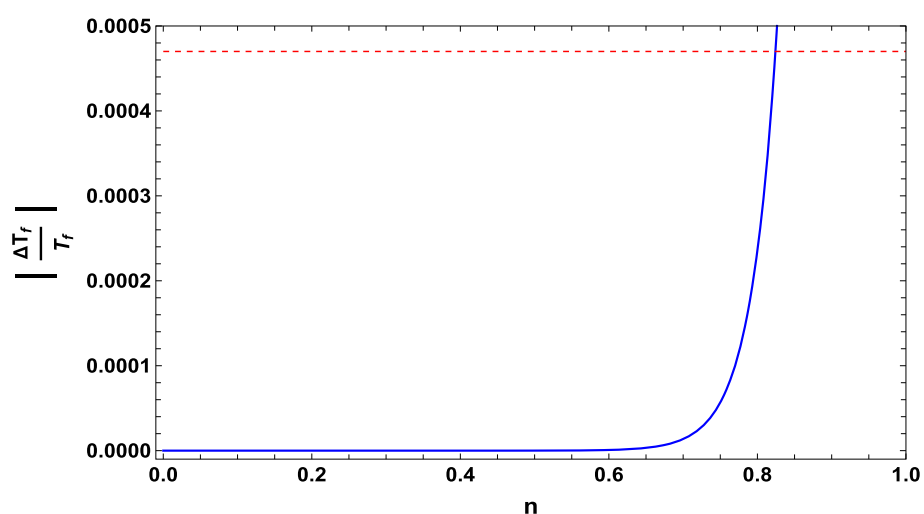


Fig. 7 Variation of $\left| \frac{\Delta T_f}{T_f} \right|$ given in Eq. (61) against free parameter n



Substituting the transformation from t to z and differentiating w.r.t. redshift z , simplification leads to the relation

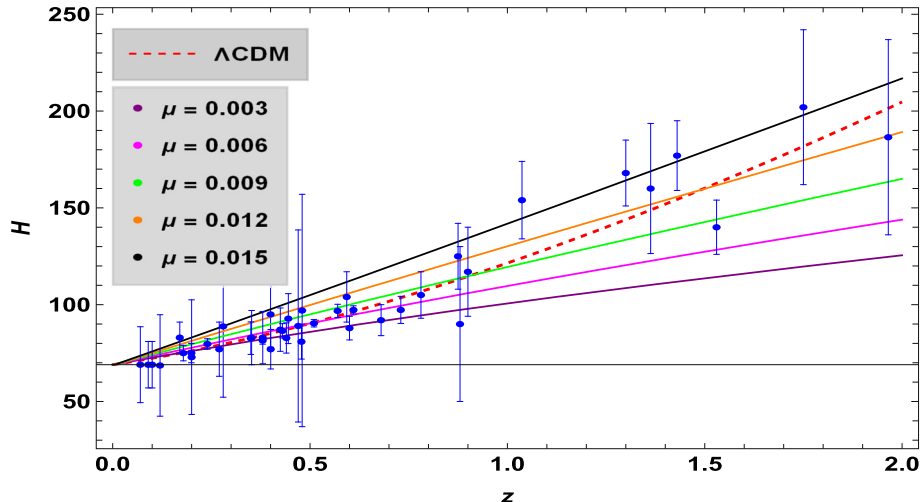
$$\begin{aligned} \alpha(1-6n)[3H^2(-3\lambda+6\mu+1)-6\mu(z+1)H(z)H'] \\ -3H_0^2\Omega(z+1)^{3(\omega+1)}+6\alpha\mu(n-1)nH(-3(z+1)H^2 \\ \times(-3\lambda+6\mu+1)H')\left(6\mu(z+1)^3HH''-6(z+1)H^2\right. \\ \times(-3\lambda+6\mu+1)H'+12\mu(z+1)^2HH' \\ \left.-6\mu(z+1)H^2H'+(z+1)^2HH'^2\right)=0. \quad (63) \end{aligned}$$

The above equation is a complicated second order differential equation from which it is difficult to obtain the exact solution. To overcome this complexity, we solve this equation numerically by using the software mathematica and extracted 43 different values of H against z given in serial number 1 to 43 in Table 1 and plot them in Fig. 8 for different choices of the parameter μ . The error bars representing observations given in [83] are also added to the figure for comparison. The estimated values for different parameters for minimum χ^2 are computed as $H_0 = 69$, $H'(0) = 1$, $\lambda = 0.31$, $\omega = -1/3$, $\Omega_{DE0} = 0.7$ which are same as the values chosen to plot Fig. 7 with five different values of μ mentioned in the panel. The values of χ^2 obtained for different values of μ are

$$\chi^2 = \begin{cases} 80.0307 & \text{for } \mu = 0.003, \\ 41.7924 & \text{for } \mu = 0.006, \\ 59.4275 & \text{for } \mu = 0.009, \\ 141.9066 & \text{for } \mu = 0.012, \\ 295.6098 & \text{for } \mu = 0.015. \end{cases}$$

To test the goodness of fit for the curves (the Chi-square test), we find that the value of Hubble parameter are closed to the observations [83] when $\mu = 0.006$ and 0.009 while differ utmost from the observations when $\mu = 0.015$. It can be seen from the χ^2 analysis that the values of model parameters ($H_0 = 69$, $H'(0) = 1$, $\lambda = 0.31$, $\omega = -1/3$, $\Omega_{DE0} = 0.7$) estimate best to analyze BBN compatibility with the observational data and the Λ CDM regime.

Fig. 8 Graph Hubble parameter H against redshift z for different values of $\mu = 0.003$ (purple), 0.006 (magenta), 0.009 (green), 0.012 (orange), 0.015 (black). The dashed red line relates to the Λ CDM regime. The error bars represent the observational values. In plotting the figures, we have chosen $H_0 = 69$, $H'(0) = 1$, $\lambda = 0.31$, $\omega = -1/3$, $\Omega_{DE0} = 0.7$ and α is given in Eq. (60)



6.2 Model 2

The second model which we use to investigate BBN constraints under the realm of modified Hořava–Lifshitz gravity is

$$F(\tilde{R}) = \alpha \tilde{R} + \beta \tilde{R}^n, \quad (64)$$

where α and β are real constants. During BBN era when DM does not exist, the value of constant β can be obtained as

$$\beta = -\frac{(3\lambda - 2\mu - 1)(2\mu - 3\lambda + 1)^{-n} \left(\alpha(3\lambda - 1) - M_p^2 \Omega_{DE0} \right)}{3^{n-1} [1 - 3\lambda + 2\mu + 2n(3\lambda + \mu(3 - 4n) - 1)] H_0^{2(n-1)}}. \quad (65)$$

Inserting Eqs. (64) and (65) into (25), the simplification of Eq. (39) yields

$$\begin{aligned} \frac{\Delta T_f}{T_f} = & (10c_q M_p^2 \xi T_f^7)^{-1} [\alpha(3\lambda - 1)\xi^2 T_f^4 \\ & - H_0^2 (H_0^2(-3\lambda + 2\mu + 1))^{-n} (-3\alpha\lambda + \alpha \\ & + M_p^2 \Omega_{DE0})(\xi^2 T_f^4 (-3\lambda + 2\mu + 1))^n]. \end{aligned} \quad (66)$$

In Fig. 9, we present the graph of $\left| \frac{\Delta T_f}{T_f} \right|$ versus free parameter n with an upper bound given in (40). It can be observed from the figure that the mathematical relation (66) satisfies the upper bound for $n \leq 0.824$. The fixed parameters to plot the figure are chosen as $H_0 = 0.69$, $\lambda = 0.334$, $\mu = 0.0001$ and $\alpha = 0.001$. Moreover, the bound existing in (39) presents Λ CDM regime if we restrict n near zero. For comparison with recent observational data, we substitute ρ from continuity equation and \tilde{R} from Eq. (27) in (25), we have

$$\begin{aligned} 6nH\mu\beta(n-1)\tilde{R}^{n-2} [6(1-3\lambda+6\mu)H\dot{H}+6\mu\ddot{H}] \\ -6[(1-3\lambda+3\mu)H^2+\mu\dot{H}](\alpha+n\beta\tilde{R}^{n-1}) \\ +\alpha\tilde{R}+\beta\tilde{R}^n = \rho_0 a^{-3(1+\omega)}. \end{aligned} \quad (67)$$

Substituting the transformation from t to z and differentiating w.r.t redshift z , simplification leads to the relation

$$\begin{aligned} 6n\beta H(H(3\lambda - 3\mu - 1) + \mu(z+1)H') \\ \times \left[3H^2(6\mu - 3\lambda + 1) - 6\mu(z+1)HH' \right]^{n-1} - H_0^2 \\ \times 3\Omega_{DE0}(z+1)^{3(\omega+1)} - 6\alpha H(H(3\mu - 3\lambda + 1) \\ - \mu(z+1)H') + \beta H(3H(6\mu 3\lambda + 1) \\ - 6\mu(z+1)H') + 3\alpha H(H(-3\lambda + 6\mu + 1) \\ - 2\mu(z+1)H') + 36n\beta\mu H(n-1)(3H^2 \\ \times (-3\lambda + 6\mu + 1) - 6\mu(z+1)HH')^{n-2} \\ \times \left[6\mu(z+1)^3 HH'' - H^2(z+1)(6\mu - 3\lambda + 1)H' \right. \\ \left. + (z+1)^2 HH'^2 + 2(z+1)^2 HH' - (z+1)H^2 H' \right] = 0. \end{aligned} \quad (68)$$

We solved the above equation numerically using the software mathematica due to its complexity and calculated first 43 values of H against z listed in serial number 1 to 43 in Table 1 and plotted in Fig. 10. The error bars representing observations given in [83] are also added to the figure for comparison. The estimated values for different parameters for minimum χ^2 have been computed as $H'(0) = 1$, $\lambda = 0.334$, $\mu = 0.0001$ and $\alpha = 0.001$, $\omega = -1/3$, $\Omega_{DE0} = 0.7$ and β is given in Eq. (65) for five different values of $H_0 = 60$ (purple), 63 (magenta), 66 (green), 69 (orange), 72 (black). The values of χ^2 obtained for different values of H_0 as follows

$$\chi^2 = \begin{cases} 65.1115 & \text{for } H_0 = 60, \\ 38.7577 & \text{for } H_0 = 63, \\ 105.4443 & \text{for } H_0 = 66, \\ 223.1631 & \text{for } H_0 = 69, \\ 406.6963 & \text{for } H_0 = 72. \end{cases}$$

Fig. 9 Variation of $\left| \frac{\Delta T_f}{T_f} \right|$ given in (66) against free parameter n for the model $F(\tilde{R}) = \alpha \tilde{R} + \beta \tilde{R}^n$ in the Modified Hořava–Lifshitz cosmology

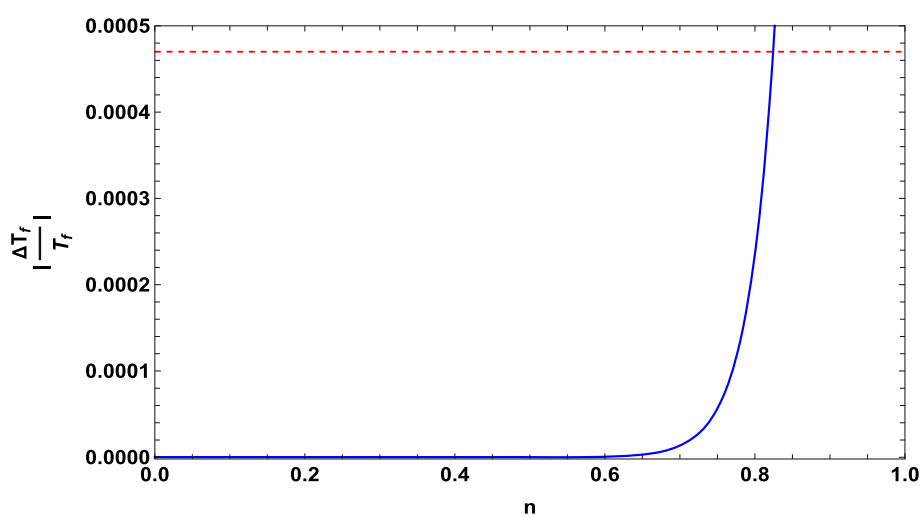
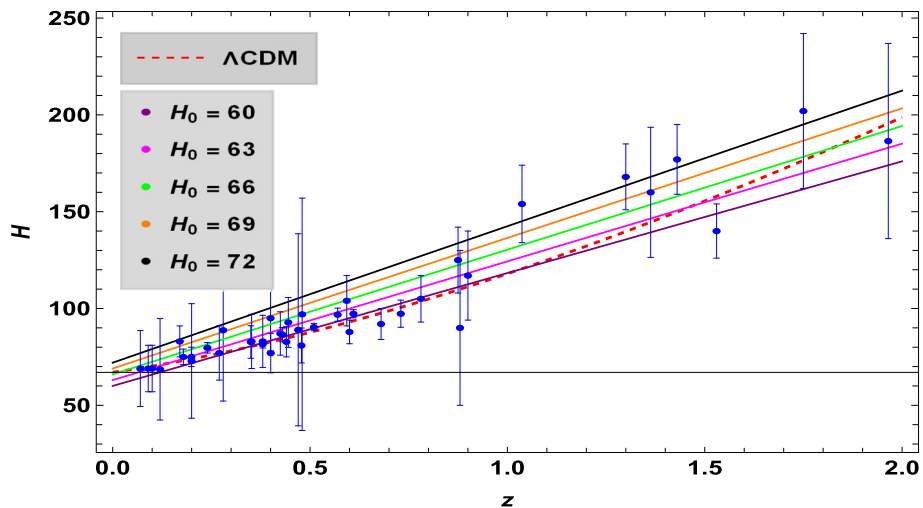


Fig. 10 Hubble parameter versus redshift error bar plot comparing with Λ CDM



The Chi-square analysis (to test the goodness of fit for the curves) gives that the obtained results are closed to the observations [83] when $H_0 = 63$ and differ utmost from the observational data when $H_0 = 72$. It is easy to deduct from the χ^2 analysis that the values of model parameters $H'(0) = 1$, $\lambda = 0.334$, $\mu = 0.0001$ and $\alpha = 0.001$, $\omega = -1/3$, $\Omega_{DE0} = 0.7$ estimate best to analyze BBN compatibility with the observational data and the Λ CDM regime.

7 Concluding remarks

In this paper, BBN phenomenon has been investigated in Einstein-Aether and modified Hořava–Lifshitz theories of gravity in the presence of observational bounds on the primordial abundance of 4He . These theories efficiently describe the late time accelerated expansion of the universe and do not spoil the behavior of early universe, particularly BBN era. Firstly, we have investigated BBN for three different models of Einstein-Aether gravity. We have attained the

BBN bound $\left| \frac{\Delta T_f}{T_f} \right| < 4.7 \times 10^{-4}$ as per recent observations for $F(K) = f_0 K^n$ (with $n \leq 0.824$), $F(K) = \alpha K^n + \beta$ (with $n \leq 0.752$) and $F(K) = K + \alpha K^2 + \beta K^n$ (with $n \leq 0.807$, $\gamma = 0.002$ and $\alpha = 10^{-9}$) as shown in Figs. 1, 3 and 5 respectively. It is of great interest that all three models described the Λ CDM regime for free parameter $n \rightarrow 0$. Moreover, Chi-square analysis has been performed for the same three models to estimate the values of model parameters and have been plotted in Figs. 2, 4 and 6 along with error bars of observational data [83]. The estimated values of the parameters for the model $F(K) = f_0 K^n$ are $H_0 = 0.69$, $M = 5$, $\gamma = 1$, for the model $F(K) = \alpha K^n + \beta$ are $n = 1.096$, $M = 5$, $\beta = 0.6$, $\gamma = 1$ and for the model $F(K) = K + \alpha K^2 + \beta K^n$ are $H_0 = 0.69$, $\alpha = 10^{-9}$, $M = 1.2$, $\gamma = 0.002$. Chi-square test showed that obtained results of Hubble parameter H are very near to the observational data.

Secondly, we have investigated BBN phenomenon for two models of modified Hořava–Lifshitz gravity. We have obtained BBN bound for both models $F(\tilde{R}) = \alpha \tilde{R}^n$ (with $n \leq 0.824$) and $F(\tilde{R}) = \alpha \tilde{R} + \beta \tilde{R}^n$ (with $n \leq 0.824$) as

shown in Figs. 7 and 9, respectively. Moreover, both models described Λ CDM regime if we restrict the free parameter n near zero. Additionally, Chi-square has computed for the same two models for an estimation of parameters values existing in the model which have been plotted in Figs. 8 and 10. The error bars of observational data are also mentioned in these plots. The estimated values of the parameters for the model $F(\tilde{R}) = \alpha \tilde{R}^n$ are $H_0 = 69$, $H'(0) = 1$, $\lambda = 0.31$ and for the model $F(\tilde{R}) = \alpha \tilde{R} + \beta \tilde{R}^n$ are $H'(0) = 1$, $\lambda = 0.334$, $\mu = 0.0001$, $\alpha = 0.001$.

In Figs. 1, 3, 5, 7 and 9, it can be seen $\left| \frac{\Delta T_f}{T_f} \right|$ (presented in blue curve) remained less than 4.7×10^{-4} (given in red line) up to some values of free parameter n for each model belonging to Einstein-Aether and modified Hořava-Lifshitz theories of gravity. This $\left| \frac{\Delta T_f}{T_f} \right| < 4.7 \times 10^{-4}$ confirms the primordial abundance of Helium (^4He) which is a confirmation to the idea of photon (light-element) production in the early history of universe. In Figs. 2, 4, 6, 8 and 10, the Chi-square test confirms the estimation of parameter values presented in the models of Einstein-Aether and modified Hořava-Lifshitz theories. In future, we can study the effects of Einstein-Aether and modified Hořava-Lifshitz theories of gravity on the primordial gravitational wave backgrounds. Since its observational evidence of number of existing polarizations are a successful tool for testing GR and extended theories of gravity. We expect that our contribution will be a source for cosmologists to explore more about BBN as it is an interesting addition in modified theories of gravity.

Acknowledgements AMS acknowledges the partial support of the University of Okara under Grant. no. UO/R/2021/6774.

Data Availability Statement This manuscript has no associated data or the data will not be deposited. [Authors' comment: This work is theoretical, so no data has been generated or analyzed. Hence, data sharing is not applicable in this manuscript.]

Open Access This article is licensed under a Creative Commons Attribution 4.0 International License, which permits use, sharing, adaptation, distribution and reproduction in any medium or format, as long as you give appropriate credit to the original author(s) and the source, provide a link to the Creative Commons licence, and indicate if changes were made. The images or other third party material in this article are included in the article's Creative Commons licence, unless indicated otherwise in a credit line to the material. If material is not included in the article's Creative Commons licence and your intended use is not permitted by statutory regulation or exceeds the permitted use, you will need to obtain permission directly from the copyright holder. To view a copy of this licence, visit <http://creativecommons.org/licenses/by/4.0/>.

Funded by SCOAP³. SCOAP³ supports the goals of the International Year of Basic Sciences for Sustainable Development.

References

1. S. Capozziello, G. Lambiase, Open problems in gravitational physics. *Frascati Phys. Ser.* **58**, 17 (2014)
2. A.G. Riess et al., Observational evidence from supernovae for an accelerating universe and a cosmological constant. *Astron. J.* **116**, 1009 (1998)
3. S. Perlmutter et al., Measurements of H_0 and Ω_m from 42 high-redshift supernovae. *Astrophys. J.* **517**, 565 (1999)
4. D.N. Spergel et al., First year Wilkinson microwave anisotropy probe (WMAP) observations: determination of cosmological parameters. *Astrophys. J. Suppl. Ser.* **148**, 175 (2003)
5. D.N. Spergel et al., Wilkinson microwave anisotropy probe (WMAP) three year results: implications for cosmology. *Astrophys. J. Suppl.* **170**, 377 (2007)
6. M. Tegmark et al., Cosmological parameters from SDSS and WMAP. *Phys. Rev. D* **69**, 103501 (2004)
7. K. Abazajian et al., The second data release of the Sloan Digital Sky Survey. *Astron. J.* **128**, 502 (2004)
8. W. Hu, S. Dodelson, Cosmic microwave background anisotropies. *Annu. Rev. Astron. Astrophys.* **40**, 171 (2002)
9. A. Jawad, A.M. Sultan, Cosmic consequences of Kaniadakis and generalized Tsallis holographic dark energy models in the fractal universe. *Adv. High Energy Phys.* **5519028**, 1 (2021)
10. S. Rani et al., Cosmographic and thermodynamic analysis of Kaniadakis holographic dark energy. *Int. J. Mod. Phys. D* **31**, 2250078 (2022)
11. E. Hubble, A relation between distance and radial velocity among extra-galactic nebulae. *Proc. Natl. Acad. Sci.* **15**, 168 (1929)
12. H.A. Bethe, Energy production in stars. *Phys. Rev.* **55**, 434 (1939)
13. S. Capozziello, G. Lambiase, E.N. Saridakis, Constraining $f(T)$ teleparallel gravity by big bang nucleosynthesis. *Eur. Phys. J. C* **77**, 576 (2017)
14. A. Ghoshal, G. Lambiase, Constraints on Tsallis cosmology from big bang nucleosynthesis & dark matter freeze-out (2021). [arXiv:2104.11296v1](https://arxiv.org/abs/2104.11296v1) [astro-ph.CO]
15. K.S. Stelle, Renormalization of higher-derivative quantum gravity. *Phys. Rev. D* **16**, 953 (1977)
16. A. Addazi et al., Quantum gravity phenomenology at the dawn of the multi-messenger era—a review. *Prog. Part. Nucl. Phys.* **125**, 103948 (2022)
17. A.A. Starobinsky, A new type of isotropic cosmological models without singularity. *Phys. Lett. B* **91**, 99 (1980)
18. P.D. Mannheim, D. Kazanas, Exact vacuum solution to conformal Weyl gravity and galactic rotation. *Astrophys. J.* **342**, 635 (1989)
19. A.M. Sultan, A. Jawad, Dynamic study of Weyl tensor corrected $f(R)$ gravity. *Int. J. Geom. Methods Mod. Phys.* **19**(03), 2250034 (2022)
20. D. Lovelock, The Einstein tensor and its generalizations. *J. Math. Phys.* **12**, 498 (1971)
21. A. Nicolis, R. Rattazzi, E. Trincherini, Galileon as a local modification of gravity. *Phys. Rev. D* **79**, 064036 (2009)
22. C. Deffayet, G. Esposito-Farese, A. Vikman, Covariant galileon. *Phys. Rev. D* **79**, 084003 (2009)
23. P. Bueno, P.A. Cano, Einsteinian cubic gravity. *Phys. Rev. D* **94**, 104005 (2016)
24. C. Erices, E. Papantonopoulos, E.N. Saridakis, Cosmology in cubic and $f(P)$ gravity. *Phys. Rev. D* **99**, 123527 (2019)
25. S. Nojiri, S.D. Odintsov, *Int. J. Geom. Methods Mod. Phys.* **4**, 115 (2007)
26. S. Capozziello, M. De Laurentis, Extended theories of gravity. *Phys. Rep.* **509**, 167 (2011)
27. V. Faraoni, S. Capozziello, Beyond Einstein gravity: a survey of gravitational theories for cosmology and astrophysics. *Fundamental Theories of Physics*, vol 170. Springer (2011)
28. K. Bamba, S.D. Odintsov, Inflationary cosmology in modified gravity theories. *Symmetry* **7**, 220 (2015)
29. Y.F. Cai et al., $f(T)$ teleparallel gravity and cosmology. *Rep. Prog. Phys.* **79**, 106901 (2016)

30. S. Nojiri, S.D. Odintsov, V.K. Oikonomou, Modified gravity theories on a nutshell: inflation, bounce and late-time evolution. *Phys. Rep.* **692**, 1 (2017)

31. K. Bamba et al., Dark energy cosmology: the equivalent description via different theoretical models and cosmography tests. *Astrophys. Space Sci.* **342**, 155 (2012)

32. A. Wang, D. Wands, R. Maartens, *JCAP* **03**, 013 (2010)

33. A. Wang, R. Maartens, *Phys. Rev. D* **81**, 024009 (2010)

34. A. Wang, Y. Wu, *JCAP* **07**, 012 (2009)

35. C. Bogdanos, E.N. Saridakis, *Class. Quantum Gravity* **27**, 075005 (2010)

36. E.N. Saridakis, *Eur. Phys. J. C* **67**, 229 (2010)

37. E.N. Saridakis, P.F. Gonzalez-Diaz, C.L. Siguenza, *Class. Quantum Gravity* **26**, 165003 (2009)

38. E.N. Saridakis, *Nucl. Phys. B* **819**, 116 (2009)

39. E.N. Saridakis, *Phys. Lett. B* **660**, 138 (2008)

40. E.N. Saridakis, *Phys. Lett. B* **661**, 335 (2008)

41. E.N. Saridakis, *Phys. Lett. B* **676**, 7 (2009)

42. M.R. Setare, E.N. Saridakis, *JCAP* **0903**, 002 (2009)

43. M.R. Setare, E.N. Saridakis, *Phys. Lett. B* **671**, 331 (2009)

44. M.R. Setare, *Phys. Lett. B* **671**, 331 (2009)

45. G. Lambiase, G. Scarpetta, *Phys. Rev. D* **74**, 087504 (2006)

46. V.K. Oikonomou, *Int. J. Geom. Methods Mod. Phys.* **13**, 1650033 (2016)

47. V.K. Oikonomou, E.N. Saridakis, *Phys. Rev. D* **94**, 124005 (2016)

48. S.D. Odintsov, V.K. Oikonomou, *Europhys. Lett.* **116**, 49001 (2016)

49. S.D. Odintsov, V.K. Oikonomou, *Phys. Lett. B* **760**, 259 (2016)

50. A. Jawad et al., Thermodynamic implications of multi-quintessence scenario. *Entropy* **21**, 851 (2019)

51. A. Jawad, Z. Khan, S. Rani, Cosmological and thermodynamics analysis in Weyl gravity. *Eur. Phys. J. C* **80**, 71 (2020)

52. A. Jawad et al., Cosmological aspects of sound speed parameterizations in fractal universe. *Eur. Phys. J. C* **79**, 926 (2019)

53. S. Rani, M.B.A. Sulehri, A. Jawad, Cosmological consequences of parameterized $f(R, \nabla R)$ gravity. *Phys. Dark Universe* **29**, 100555 (2020)

54. J.D. Barrow, S. Basilakos, E.N. Saridakis, Big bang nucleosynthesis constraints on Barrow entropy. *Phys. Lett. B* **815**, 136134 (2021)

55. S. Bhattacharjee, BBN constraints on $f(Q, T)$ gravity. *Int. J. Mod. Phys. A* **37**(06), 2250017 (2022)

56. P. Asimakis et al., Big bang nucleosynthesis constraints on higher-order modified gravities. *Phys. Rev. D* **105**, 084010 (2022)

57. E.W. Kolb, M.S. Turner, *The Early Universe* (Addison Wesley Publishing Company, Boston, 1989)

58. J. Bernstein, L.S. Brown, G. Feinberg, Cosmological Helium production simplified. *Rev. Mod. Phys.* **61**, 25 (1989)

59. B.D. Fields et al., Big-bang nucleosynthesis after Planck. *JCAP* **03**, 010 (2020)

60. T. Jacobson, D. Mattingly, Gravity with a dynamical preferred frame. *Phys. Rev. D* **64**, 024028 (2001)

61. S. Carloni et al., Modified first-order Hořava–Lifshitz gravity: Hamiltonian analysis of the general theory and accelerating FRW cosmology in a power-law $F(R)$ model. *Phys. Rev. D* **85**, 129904 (2012)

62. S. Rani et al., Thermodynamics in modified Brans–Dicke gravity with entropy corrections. *Eur. Phys. J. C* **78**, 58 (2018)

63. M. Gasperini, Repulsive gravity in the very early Universe. *Gen. Relativ. Gravit.* **30**, 1703 (1998)

64. T.G. Zlosnik, P.G. Ferreira, G.D. Starkman, Modifying gravity with the Aether: an alternative to Dark Matter. *Phys. Rev. D* **75**, 044017 (2007)

65. S. Rani et al., Cosmological consequences of new dark energy models in Einstein–Aether gravity. *Symmetry* **11**, 509 (2019)

66. M. Chaichian et al., Corrigendum: Modified $F(R)$ Hořava–Lifshitz gravity: a way to accelerating FRW cosmology. *Class. Quantum Gravity* **29**, 159501 (2012)

67. J. Kluson, New models of $f(R)$ theories of gravity. *Phys. Rev. D* **81**, 064028 (2010)

68. S. Mukohyama, Dark matter as integration constant in Hořava–Lifshitz gravity. *Phys. Rev. D* **80**, 064005 (2009)

69. A.G. Cohen, A. Rujula, S.L. De Glashow, A matter–antimatter universe? *ApJ* **495**, 539 (1998)

70. K.A. Olive, G. Steigman, T.P. Walker, Primordial nucleosynthesis: theory and observations. *Phys. Rep.* **333**, 389 (2000)

71. R.H. Cyburt et al., Big bang nucleosynthesis: present status. *Phys. Rev. Mod. Phys.* **88**, 015004 (2016)

72. D.F. Torres, H. Vucetich, A. Plastino, Early universe test of nonextensive statistics. *Phys. Rev. Lett.* **79**, 1588 (1997)

73. G. Lambiase, Dark matter relic abundance and big bang nucleosynthesis in Hořava’s gravity. *Phys. Rev. D* **83**, 107501 (2011)

74. K.A. Olive et al., Review of particle physics. *Chin. Phys. C* **38**, 0900001 (2014)

75. G. Lambiase, Lorentz invariance breakdown and constraints from big-bang nucleosynthesis. *Phys. Rev. D* **72**, 087702 (2005)

76. K.A. Olive, E. Skillman, G. Steigman, The primordial abundance of 4He : an update. *Astrophys. J.* **483**, 788 (1997)

77. Y.I. Izotov, T.X. Thuan, The primordial abundance of 4He revisited. *Astrophys. J.* **500**, 188 (1998)

78. B.D. Fields, K.A. Olive, On the evolution of helium in blue compact galaxies. *Astrophys. J.* **506**, 177 (1998)

79. D. Kirkman et al., The cosmological baryon density from the deuterium-to-hydrogen ratio in QSO absorption systems: D/H toward Q1243+3047. *Astrophys. J. Suppl. Ser.* **149**, 1 (2003)

80. A. Coc et al., Updated big bang nucleosynthesis compared with Wilkinson Microwave Anisotropy Probe observations and the abundance of light elements. *Astrophys. J.* **600**, 544 (2004)

81. Y.I. Izotov, T.X. Thuan, Systematic effects and a new determination of the primordial abundance of 4He and dY/dZ from observations of blue compact galaxies. *Astrophys. J.* **602**, 200 (2004)

82. K. Pearson, On the criterion that a given system of deviation from the probable in the case of a correlated system of variables is such that it can be reasonably supposed to have arisen from sampling. *Philos. Mag. (5)* **50**, 157 (1900)

83. V.K. Bhardwaj et al., An axially symmetric transitioning models with observational constraints (2022). [arXiv:2204.04451v1 \[gr-qc\]](https://arxiv.org/abs/2204.04451v1)

84. E. Macaulay et al., First cosmological results using Type Ia supernovae from the Dark Energy Survey: measurement of the Hubble constant. *Mon. Not. R. Astron. Soc.* **486**, 2184 (2019)

85. C. Zhang et al., Four new observational $H(z)$ data from luminous red galaxies in the Sloan Digital Sky Survey data release seven. *Res. Astron. Astrophys.* **14**, 1221 (2014)

86. J. Simon, L. Verde, R. Jimenez, Constraints on the redshift dependence of the dark energy potential. *Phys. Rev. D* **71**, 123001 (2005)

87. D. Stern et al., Cosmic chronometers: constraining the equation of state of dark energy. I: $H(z)$ measurements. *JCAP* **1002**, 008 (2010)

88. M. Moresco et al., Improved constraints on the expansion rate of the Universe up to $z \sim 1.1$ from the spectroscopic evolution of cosmic chronometers. *JCAP* **2012**, 006 (2012)

89. E.G. Naga et al., Clustering of luminous red galaxies IV. Baryon acoustic peak in the line-of-sight direction and a direct measurement of $H(z)$. *Mon. Not. R. Astron. Soc.* **399**, 1663 (2009)

90. S. Alam et al., The clustering of galaxies in the completed SDSS-III Baryon Oscillation Spectroscopic Survey: cosmological analysis of the DR12 galaxy sample. *Mon. Not. R. Astron. Soc.* **470**, 2617 (2017)

91. D.H. Chauang, Y. Wang, Modelling the anisotropic two-point galaxy correlation function on small scales and single-probe mea-

surements of $H(z)$, $DA(z)$ and $f(z)\sigma 8(z)$ from the Sloan Digital Sky Survey DR7 luminous red galaxies. *Mon. Not. R. Astron. Soc.* **435**, 255 (2013)

92. M. Moresco et al., A 6% measurement of the Hubble parameter at $z \sim 0.45$ direct evidence of the epoch of cosmic re-acceleration. *JCAP* **05**, 014 (2016)
93. C. Blake et al., The Wiggle Z Dark Energy Survey: joint measurements of the expansion and growth history. *Mon. Not. R. Astron. Soc.* **425**, 405 (2012)
94. A.L. Ratsimbazafy et al., Age-dating luminous red galaxies observed with the Southern African Large Telescope. *Mon. Not. R. Astron. Soc.* **467**, 3239 (2017)
95. P. Sarmah, U.D. Goswami, Bianchi Type I model of universe with customized scale factors. *Mod. Phys. Lett. A* **37**(21), 2050134 (2022). [arXiv:2203.00385](https://arxiv.org/abs/2203.00385)
96. M. Moresco, Raising the bar: new constraints on the Hubble parameter with cosmic chronometers at $z \equiv 2$. *Mon. Not. R. Astron. Soc.* **450**, L16 (2015)
97. N.G. Busa et al., Baryon acoustic oscillations in the Ly α forest of BOSS quasars. *Astron. Astrophys.* **552**, A96 (2013)
98. T. Delubac et al., Baryon acoustic oscillations in the Ly α forest of BOSS DR11 quasars. *Astron. Astrophys.* **574**, A59 (2015)
99. A. Font-Ribera et al., Quasar-Lyman α forest cross-correlation from BOSS DR11: Baryon Acoustic Oscillations. *JCAP* **2014**, 027 (2014)
100. C. Ranjit, P. Rudra, S. Kundu, Dynamical system analysis of modified chaplygin gas in Einstein-Aether gravity. *Eur. Phys. J. Plus* **129**, 208 (2014)
101. R.C. Nunes, S. Pan, E.N. Saridakis, New observational constraints on $f(T)$ gravity from cosmic chronometers. *JCAP* **1608**(08), 011 (2016)